Supporting Information

Co_3O_4/TiO_2 Catalysts Studied *In Situ* During the Preferential Oxidation of Carbon Monoxide: *The Effect of Different TiO_2 Polymorphs*

Thulani M. Nyathi,[a] Mohamed I. Fadlalla,[a] Nico Fischer,[a] Andrew P. E. York,[b] Ezra J. Olivier,[c] Emma K. Gibson,[d,e] Peter P. Wells,[e,f,g] Michael Claeys[a,*]

[a] *Catalysis Institute and c*change (DSI-NRF Centre of Excellence in Catalysis), Department of Chemical Engineering, University of Cape Town, Rondebosch 7701, South Africa*

[b] *Johnson Matthey Technology Centre, Sonning Common, Reading RG4 9NH, United Kingdom*

[c] *Centre for High Resolution Transmission Electron Microscopy, Physics Department, Nelson Mandela University, PO Box 77000, Gqeberha, 6031, South Africa*

[d] *School of Chemistry, Joseph Black Building, University of Glasgow, Glasgow G12 8QQ, United Kingdom*

[e] *UK Catalysis Hub, Research Complex at Harwell, Rutherford Appleton Laboratory, Harwell, Oxon, OX11 0FA, United Kingdom*

[f] *School of Chemistry, University of Southampton, University Road, Southampton SO17 1BJ, United Kingdom*

[g] *Diamond Light Source Ltd., Harwell Science and Innovation Campus, Chilton, Didcot OX11 0DE, United Kingdom*

Corresponding Author:

* Michael Claeys: michael.claeys@uct.ac.za

On-line gas chromatography

Table S1: Parameters set for achieving gas separation in the different modules of the micro-GC.

Channel	1	2	3
Detector type	TCD	TCD	TCD
Column type and length	Molecular Sieve 5Å PLOT, 20 m	PoraPLOT Q, 10 m	Molecular Sieve 5Å PLOT, 10 m
Injection temperature (°C)	100	100	100
Injection time (msec)	40	40	40
Carrier gas	H_2	H_2	Ar
Column temperature (°C)	80	60	80
Column pressure (kPa)	150	80	150
Duration (sec)	270	270	270
Gas(es) analysed	O_2, N_2, and CO	CH_4 and CO_2	H_2

The micro-GC (Varian CP-4900) was calibrated using two calibration gas cylinders – one having a mixture of 39.8% H_2, 18.5% CO, 15.9% CH_4, 10.1% CO_2, 9.9% Ar, and 5.8% N_2 (AFROX), and the other gas cylinder had synthetic air (21% O_2 in N_2, Air Products). From the chromatograms, response factors for each gas (except for N_2 and Ar) were calculated (see Equation S1) using N_2 as the reference, since it was present in both gas cylinders and was the only gas that would not get consumed under reaction conditions. To calculate the volumetric flow rate for each gas, Equation S2 was used.

$$F_i = \frac{A_{N_2} \cdot v_{i,\ in}}{A_i \cdot v_{N_2,\ in}} \qquad (S1)$$

$$v_{i,\ out}(mL/min) = F_i \cdot \frac{A_i \cdot v_{N_2,\ in}}{A_{N_2}} \qquad (S2)$$

F_i is the response factor of gas component i with reference to N_2. A_{N_2} is the calculated peak area of nitrogen, and A_i is the calculated peak area of gas component i. $v_{N_2,\ in}$ is the volumetric gas flow rate of nitrogen, and $v_{i,\ in}$ is the volumetric gas flow rate of gas component i entering the system during the GC calibrations or the CO-PrOx experiments. Finally, $v_{i,\ out}$ is the volumetric gas flow rate of gas component i exiting the reactor during CO-PrOx.

The performance of the catalyst was assessed by calculating normalised gas outlet flow rates (Equation S3), conversions/yields (Equations S4 and S5), and selectivities (Equation S6).

$$\bar{v_{j,out}} = \frac{v_{j,\ out}}{v_{i,\ in}} \qquad (S3)$$

$$X_{CO\rightarrow CO_2} or\ Y_{CO_2}(\%) = \frac{v_{CO,\ in} - v_{CO,\ out} - v_{CH_4,\ out}}{v_{CO,\ in}} \times 100 = \frac{v_{CO_2,\ out}}{v_{CO,\ in}} \times 100 \qquad (S4)$$

$$X_{CO\rightarrow CH_4} or\ Y_{CH_4}(\%) = \frac{v_{CO,\ in} - v_{CO,\ out} - v_{CO_2,\ out}}{v_{CO,\ in}} \times 100 = \frac{v_{CH_4,\ out}}{v_{CO,\ in}} \times 100 \qquad (S5)$$

$$S_{O_2\rightarrow CO_2}(\%) = \frac{v_{CO,\ in} - v_{CO,\ out} - v_{CH_4,\ out}}{2 \cdot \left(v_{O_2,\ in} - v_{O_2,\ out}\right)} \times 100 = \frac{v_{CO_2,\ out}}{2 \cdot \left(v_{O_2,\ in} - v_{O_2,\ out}\right)} \times 100 \qquad (S6)$$

$\bar{v_{j,out}}$ is the normalised gas outlet flow rate of gas j.

Ex situ catalyst characterisation

Powder X-ray diffraction (PXRD) measurements on the fresh supported catalysts were carried out in a Bruker D8 Advance Laboratory X-ray diffractometer equipped with a Co X-ray source ($\lambda_{K\alpha1}$ = 0.178897 nm) and a position-sensitive detector (LYNXEYE XE, Bruker AXS). The diffractometer was operated at 35 kV and 40 mA, and the optics were set to Bragg-Brentano geometry. A 2θ measurement window of 20 – 120° (or a 1/d range of 1.9 – 9.7 nm^{-1}, where "d" is the d-spacing), a step size of 0.043° (4.2 x 10^{-3} nm^{-1}), and a time per step of 0.75 s were applied (total scan time: 29 min and 50 s). We note that two different X-ray sources (one on each diffractometer) were used in the current work, *i.e.*, Co for the *ex situ* measurements and Mo ($\lambda_{K\alpha1}$ = 0.07093 nm) for the *in situ* measurements (see section 2.2. of the main paper and the section "*In situ* catalyst characterisation" in the Supporting Information). This can result in dissimilar 2θ positions (or values) for the reflections of the same crystalline phase. Therefore, we chose to plot all *ex situ* and *in situ* diffraction patterns as a function of 1/d instead of 2θ to eliminate this effect (see example in Figure S1 and the Bragg Law equation[1] (Equation S7)).

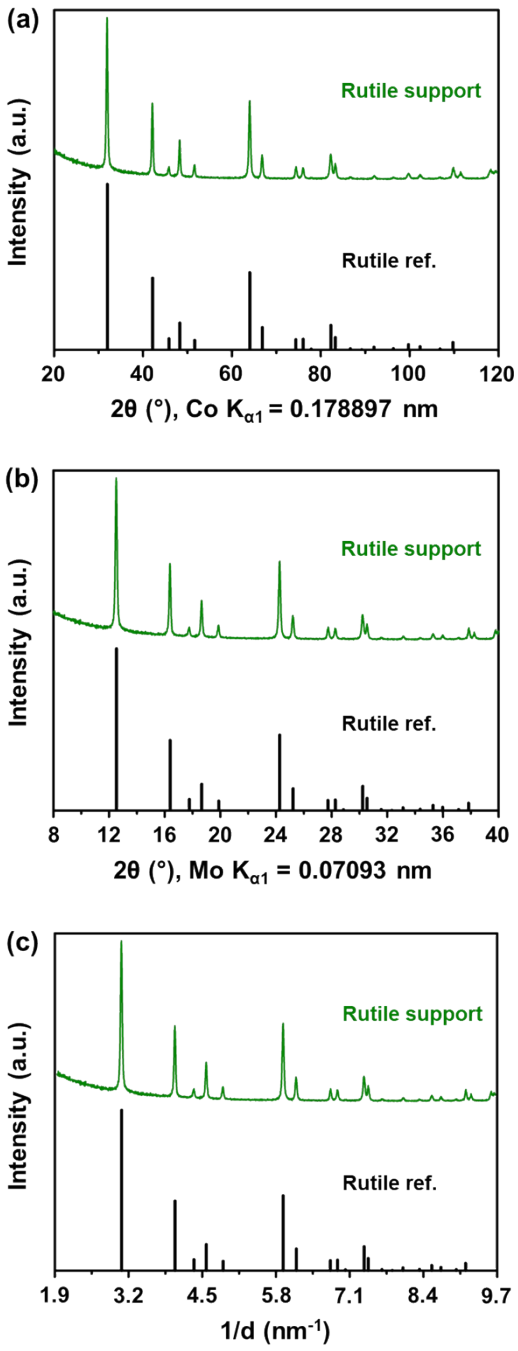

Figure S1: (a) *Ex situ* PXRD pattern of the bare Rutile support recorded using a Co X-ray source. The same PXRD pattern is replotted **(b)** as a function of the expected 2θ positions from a Mo X-ray source, and **(c)** as a function of the unifying parameter, 1/d (also see Bragg Law equation[1] - Equation S7). Note that all reflections from Rutile (see Table S2 for the ICDD PDF-2 entry) are expected to be at much lower diffraction angles when using a Mo source than when using a Co source.

$$\frac{1}{d}\left(nm^{-1}\right) = \frac{2sin\theta_{Co}}{\lambda_{Co}} = \frac{2sin\theta_{Mo}}{\lambda_{Mo}} \qquad (S7)$$

d is the interplanar distance or d-spacing, θ_{Co} and θ_{Mo} are the measured diffraction angles (normally reported as 2θ) from a PXRD instrument equipped either with a cobalt source of X-ray wavelength λ_{Co} or a molybdenum source of X-ray wavelength λ_{Mo}, respectively.

All recorded *ex situ* diffraction patterns were compared with known diffraction patterns found in the International Centre for Diffraction Data (ICDD) Powder Diffraction File-2 (PDF-2) database[2] to determine the chemical and crystallographic phases present. A summary of the PDF entries accessed can be found in Table S2. Rietveld refinement was carried out using the TOPAS 5.0 software package[3] (Bruker AXS) to quantify the Co-based phases present in terms of their relative weight fraction and volume-based average crystallite size.

Table S2: ICDD PDF-2 entries of all chemical/crystal phases relevant to the current study.

Chemical formula	Chemical name	PDF entry
α-Co	α-Cobalt (hexagonal)	01-071-4239
β-Co	β-Cobalt (cubic)	00-015-0806
CoO (cubic)	Cobalt(II) oxide (cubic)	00-043-1004
Co_3O_4	Cobalt(II,III) oxide	01-073-1701
$CoTiO_3$ (rhombohedral)	Cobalt(II) titanium(IV) oxide (rhombohedral)	00-029-0516
$CoTiO_3$ (cubic)	Cobalt(II) titanium(IV) oxide (cubic)	00-015-0866
TiO_2 (anatase)	Titanium(IV) oxide (anatase)	01-089-4921
TiO_2 (rutile)	Titanium(IV) oxide (rutile)	01-089-4202

Scanning transmission electron microscopy (STEM) was performed on all fresh and spent catalysts in a JEM-ARM200F microscope (JEOL) equipped with a field emission cathode and an integrated correction of the spherical aberrations of the objective and condenser lenses. The instrument is fitted with an advanced GIF (Gatan Image Filter) electron spectrometer with electron energy loss spectroscopy (EELS) capabilities. Lacey carbon sample grids (Agar Scientific) were utilised for the STEM analysis. Particle size measurements were carried out using the freeware ImageJ 1.15a.[4] Thereafter, the number- and volume-based average particle sizes, and the associated standard deviations were calculated using Equations S8 – S11. The STEM-derived volume-based average particle sizes can be compared with the PXRD-derived average crystallite sizes since they are also volume-based.

$$number - based\ average\ \left(\bar{d}_{c,\,n}\right) = \frac{\sum_{i=1}^{N} n_i d_i}{N} \qquad (S8)$$

$$volume - based\ average\ \left(\bar{d}_{c,\,v}\right) = \frac{\sum_{i=1}^{N} n_i d_i^4}{\sum_{i=1}^{N} n_i d_i^3} \qquad (S9)$$

$$number - based\ standard\ deviation\ \left(sd_n\right) = \sqrt{\frac{\sum_{i=1}^{N} n_i \left(d_i - \bar{d}_{c,\,n}\right)^2}{N-1}} \qquad (S10)$$

$$volume - based\ standard\ deviation\ \left(sd_v\right) = \sqrt{\frac{\sum_{i=1}^{N} n_i d_i^3 \left(d_i - \bar{d}_{c,\,v}\right)^2}{\frac{N-1}{N}\sum_{i=1}^{N} n_i d_i^3}} \qquad (S11)$$

d_i is the diameter of particle i, n_i is the number of particles of size d_i, and N is the total number of particles counted. The above equations can also be found in the book chapter by Bergeret and Gallezot.[5]

Nitrogen physisorption was conducted on all bare supports and fresh supported catalysts in a Micromeritics TriStar II 3020 after degassing the samples (*ca.* 0.3 g each) at 200 °C overnight. The mass-specific surface area of each sample was calculated using the Brunauer–Emmett–Teller (BET) method. The mass-specific pore volume was calculated by applying the Barrett-Joyner-Halenda (BJH) method.

The fresh catalysts (*ca.* 0.05 g each) for elemental analysis, performed using inductively coupled plasma-optical emission spectroscopy (ICP-OES), were pre-treated overnight in a 3:1:1 mixture of HCl:HNO_3:HF. Subsequently, the mixture was heated at a rate of 6.4 °C/min to 180 °C for 40 min for digestion in a MARS-5 microwave digester to ultimately obtain the Co loadings/concentrations in a Varian ICP-OES 730 instrument (Agilent).

X-ray absorption spectroscopy (XAS) measurements were performed at the Co K-edge (7709 eV) on beamline B18 at Diamond Light Source (United Kingdom), operating with a ring energy of 3 GeV and a ring current of 300 mA.[6] A Co foil was used for energy calibration. The scans were performed in quick extended X-ray absorption fine structure (QEXAFS) mode from 7509 to 8559 eV, with a resolution of 0.3 eV/point, and each scan was approximately 3 min. Three scans were recorded for each sample to check reproducibility and to obtain a good signal-to-noise ratio. The samples were diluted with cellulose and pressed into discs prior to being measured in transmission mode. The data processing was performed using the Athena software, which is part of the open-source software package Demeter[7] (based on the IFEFFIT library[8]). Linear combination fitting (LCF) was performed between 7675 and 7825 eV (*i.e.*, -50 eV before the edge and +100 eV after the edge). The reference spectra considered for the LCF were of Co_3O_4,[9] CoO,[10] $CoTiO_3$,[11] and Co foil.[6] These reference samples were synthesised according to the procedures outlined in the cited literature.

In situ catalyst characterisation

Reduction studies

The reduction of the supported catalysts (*ca*. 0.012 g each) was carried out in a gas flow of 50% H_2 in N_2 (1.2 mL(NTP)/min) at atmospheric pressure using a capillary-based reaction cell (developed at the University of Cape Town (UCT), South Africa).[12–14] The cell was mounted on a Bruker D8 Advance Laboratory X-ray diffractometer, equipped with a Mo X-ray source ($\lambda_{K\alpha1}$ = 0.07093 nm) and a position-sensitive detector (VANTEC, Bruker AXS), to allow for PXRD patterns to be recorded during the reduction. The diffractometer was operated at 50 kV and 35 mA, and the optics were set to parallel beam geometry to minimise possible peak shifts due to sample height differences.

The cell uses a fixed-bed capillary reactor (made of borosilicate glass, length: 75 mm, wall thickness: 0.02 mm, and O.D.: 1.0 mm (Capillary Tube Supplies LTD, UK)), through which gas can be flowed using a mass flow controller (Brooks Instruments). The loaded reactor was heated from 50 to 450 °C (at a rate of 1 °C/min), and thereafter, the temperature was held at 450 °C for 2 h. A 2θ measurement window of 15 – 30° (or a 1/d range of 3.7 – 7.3 nm^{-1}), a step size of 0.019° (4.7 x 10^{-3} nm^{-1}), and a time per step of 0.20 s were applied (total scan time: 4 min and 2 s, with an added 58-s delay between scans). PXRD patterns were recorded every 5 min throughout each reduction experiment. All recorded *in situ* diffraction patterns were compared with known diffraction patterns in the ICDD PDF-2 database[2], and Rietveld refinement was carried out using the TOPAS 5.0 software package[3] (Bruker AXS).

Conventional H_2-TPR was conducted on the bare supports and supported Co_3O_4 catalysts. A sample of 0.1 g was placed between two pieces of quartz wool in a U-shaped quartz reactor. The reduction was carried out in a Micromeritics AutoChem 2920 instrument, equipped with

a thermal conductivity detector (TCD) for measuring the H_2 consumption. The sample was firstly dried by heating the reactor from room temperature to 120 °C at a rate of 10 °C/min under a flow of Ar (10 mL(NTP)/min), and then keeping the temperature at 120 °C for 60 min. Thereafter, the temperature was decreased to 60 °C before switching the gas flow to 5% H_2 in Ar (50 mL(NTP)/min). Under this reducing gas mixture, the reactor was heated to 920 °C at a rate of 10 °C/min, which was kept for 10 min before cooling to room temperature. The H_2 consumption was measured every 0.1 min (6 s) between 60 and 920 °C after introducing the reducing gas. The degree of reduction (DoR) of Co_3O_4 to Co^0 in the TiO_2-supported catalysts was calculated based on the instrument calibration performed using different known amounts of Ag_2O (also see Equations S12 – S14).

$$Co_3O_4(s) + 4H_2(g) \rightarrow 3Co(s) + 4H_2O(g) \qquad (S12)$$

$$H_2\ consumption\ (mmol) = 2.8 \cdot 10^{-2} + A_{peak} \cdot 2.3 \cdot 10^{-1} \qquad (S13)$$

$$Degree\ of\ reduction\ (\%) = \frac{H_2\ consumption}{x \cdot n_{metal\ oxide\ loaded}} \times 100 \qquad (S14)$$

A_{peak} is the area of the peak in the chromatogram. x is the H_2:metal oxide molar ratio as shown in Equation S12. $n_{metal\ oxide\ loaded}$ is the amount (in mmol) of Co_3O_4 in the supported catalysts loaded in the H_2-TPR quartz reactor.

Catalytic evaluation

The magnetometer uses a ½-inch stainless steel fixed-bed reactor (I.D.: 9.7 mm) that is placed vertically between two pole caps of a current-controlled electro-magnet (maximum external field strength: 2 T (or 20 kOe), Bruker Analytik GmbH). PXRD patterns and magnetisation measurements (at 2 T) were recorded every 5 min in the separate *in situ* instruments. The scan parameters (*i.e.*, 2θ (or 1/d) range, step size, and time per step) used for the PXRD-based reduction studies (section 2.2.1.) were also applied for the PXRD-based CO-PrOx reactions. The data from the magnetisation measurements were used to calculate the DoR of Co_3O_4 to

Co^0 using Equation S15, which is based on quantities from a pre-determined calibration curve (Figure S2).

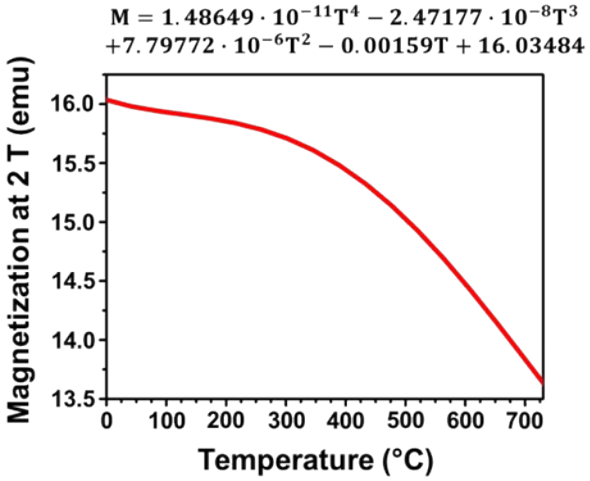

Figure S2: Calibration curve for the magnetometer based on a 0.1 g pre-reduced unsupported Co^0 sample.

$$DoR(\%) = \frac{M_{sample} \cdot 0.1}{M_{calibration} \cdot X_{loading} \cdot m_{unreduced\ sample}} \times 100 \qquad (S15)$$

M_{sample} is the sample magnetisation (in emu) at any temperature within the temperature window used in this study and $M_{calibration}$ is the corresponding magnetisation of Co^0 (in emu) from the calibration curve in Figure S2 at the same temperature. $X_{loading}$ is the metal loading as determined from ICP-OES and $m_{unreduced\ sample}$ is the mass of the unreduced supported sample (in g) loaded into the reactor.

Ex situ PXRD and STEM-EELS results for the bare supports and fresh supported catalysts

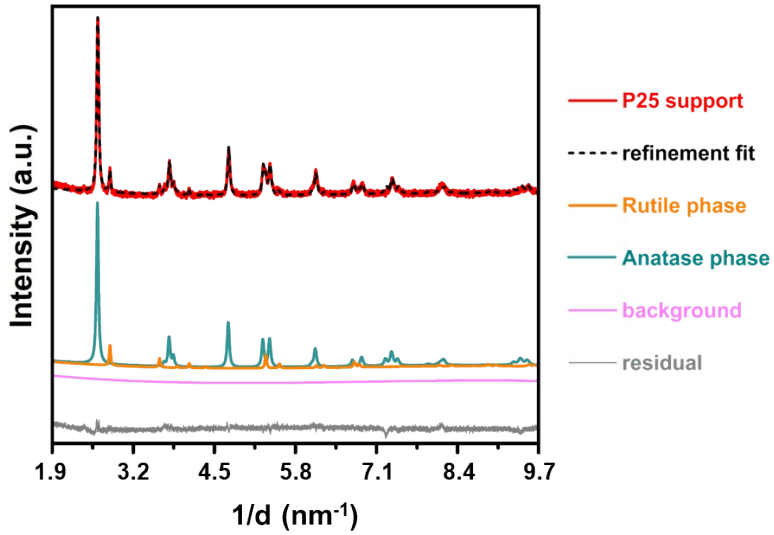

Figure S3: *Ex situ* PXRD pattern (radiation source: Co Kα1 = 0.178897 nm) of the bare P25 support. Also included are the Rietveld refinements results in terms of the fitted crystallographic phases. The Rwp value can be found in Table S3.

Table S3: Rietveld refinement results for the bare P25 support.

Sample name	**Rutile**		**Anatase**		Rwp (%)
	Crystallite size (nm)	Weight fraction (wt.-%)	Crystallite size (nm)	Weight fraction (wt.-%)	
P25 support	42.1 ± 1.8	14.7 ± 0.4	25.8 ± 1.6	85.3 ± 0.4	3.7

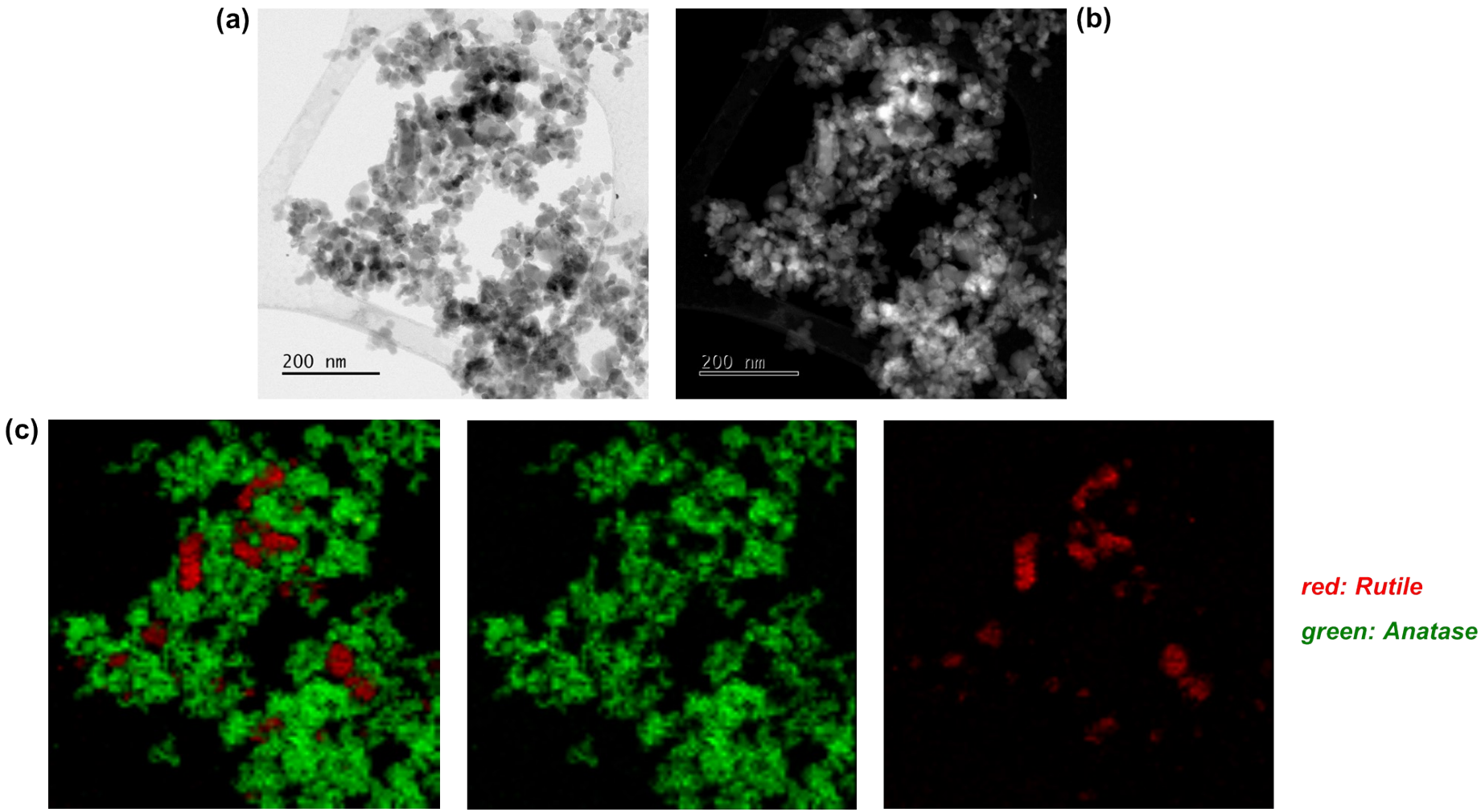

Figure S4: (a) Bright- and **(b)** dark-field STEM micrographs of the fresh Co_3O_4/P25 catalyst. **(c)** Phase composition maps derived using EELS showing the Anatase and Rutile regions in the fresh catalyst.

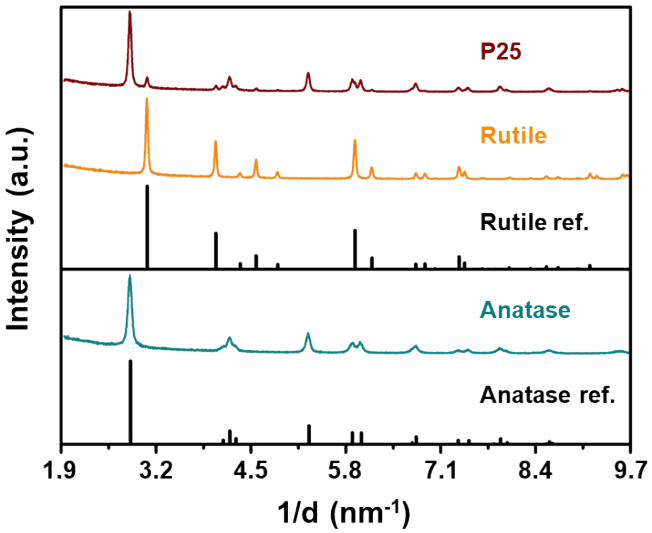

Figure S5: *Ex situ* PXRD patterns (X-ray source: Co Kα1 = 0.178897 nm) of the bare support materials and the corresponding reference reflection lines. See Table S2 for the ICDD PDF-2 entries of Rutile and Anatase.

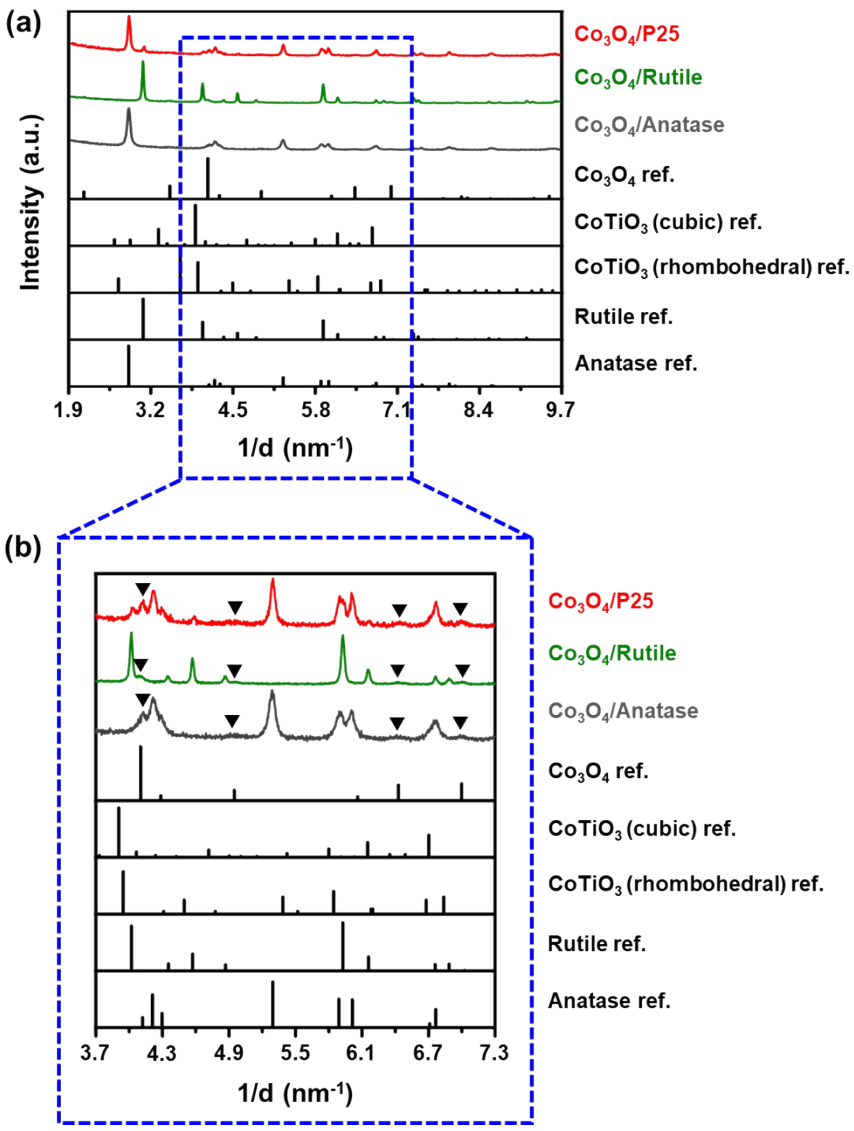

Figure S6: (a) PXRD patterns (X-ray source: Co Kα1 = 0.178897 nm) of the supported fresh samples as well as the reference reflection lines for Co_3O_4, $CoTiO_3$ (cubic and rhombohedral), Rutile, and Anatase as recorded in the ICDD PDF-2 database (see Table S2 for the PDF entries). **(b)** Magnified short 1/d range of the recorded PXRD patterns enhancing the visibility of the Co_3O_4 reflections. The black triangles indicate the identified Co_3O_4 reflections in each diffraction pattern.

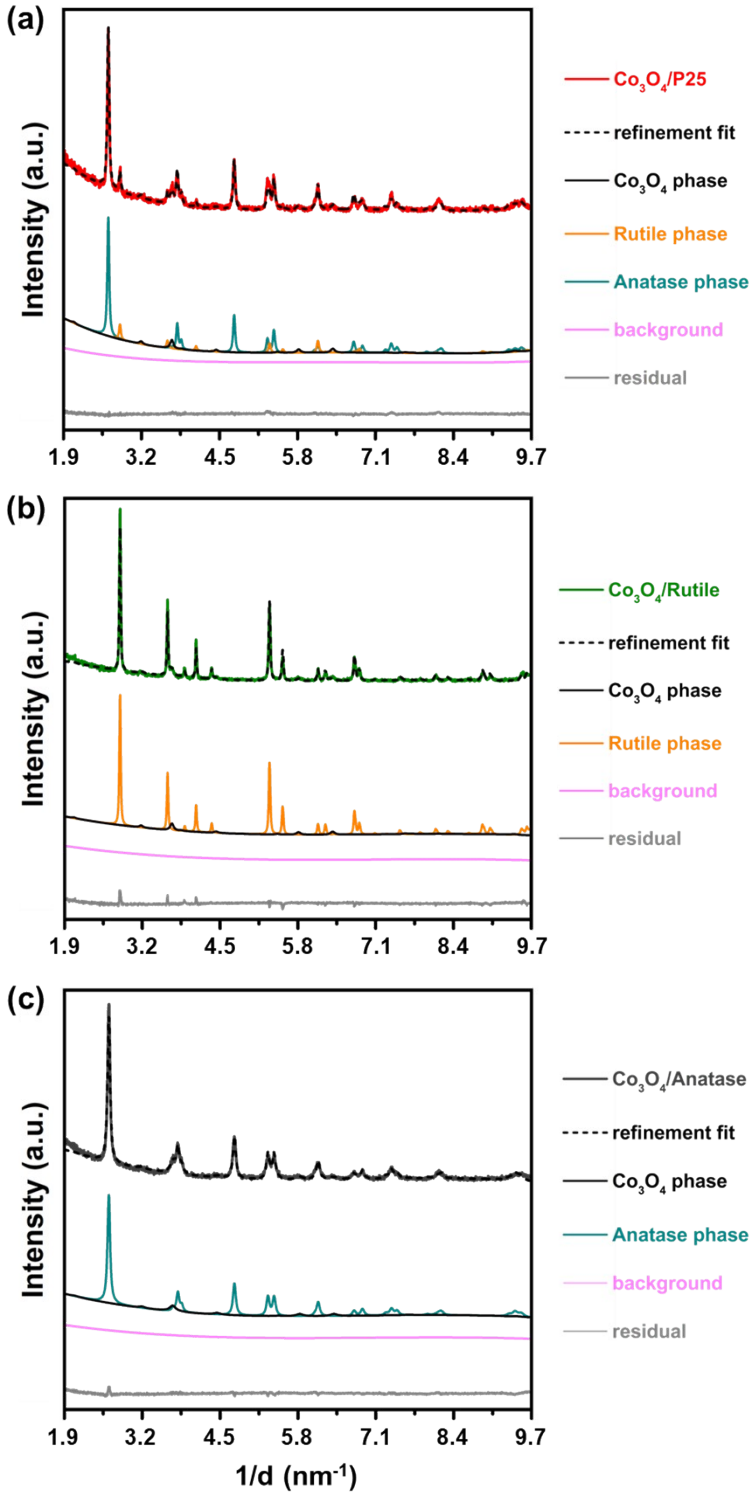

Figure S7: *Ex situ* PXRD pattern (X-ray source: Co Kα1 = 0.178897 nm) of **(a)** Co_3O_4/P25, **(b)** Co_3O_4/Rutile, and **(c)** Co_3O_4/Anatase. Also included are the Rietveld refinements results in terms of the fitted crystallographic phases. The Rwp values can be found in Table S3.

Table S4: Rietveld refinement results for the fresh supported catalysts.

Sample name	Rutile		Anatase		Co_3O_4		Rwp (%)
	Crystallite size (nm)	Weight fraction (wt.-%)	Crystallite size (nm)	Weight fraction (wt.-%)	Crystallite size (nm)	Weight fraction (wt.-%)	
Co_3O_4/P25	30.1 ± 2.1	10.5 ± 0.3	27.9 ± 0.5	79.2 ± 0.3	11.8 ± 0.3	10.3 ± 0.3	10.1
Co_3O_4/Rutile	47.9 ± 0.8	89.7 ± 0.5	-	-	14.7 ± 0.3	10.3 ± 0.5	11.4
Co_3O_4/Anatase	-	-	18.1 ± 0.3	91.5 ± 0.3	9.8 ± 0.2	8.5 ± 0.3	10.8

In situ PXRD-based reduction results

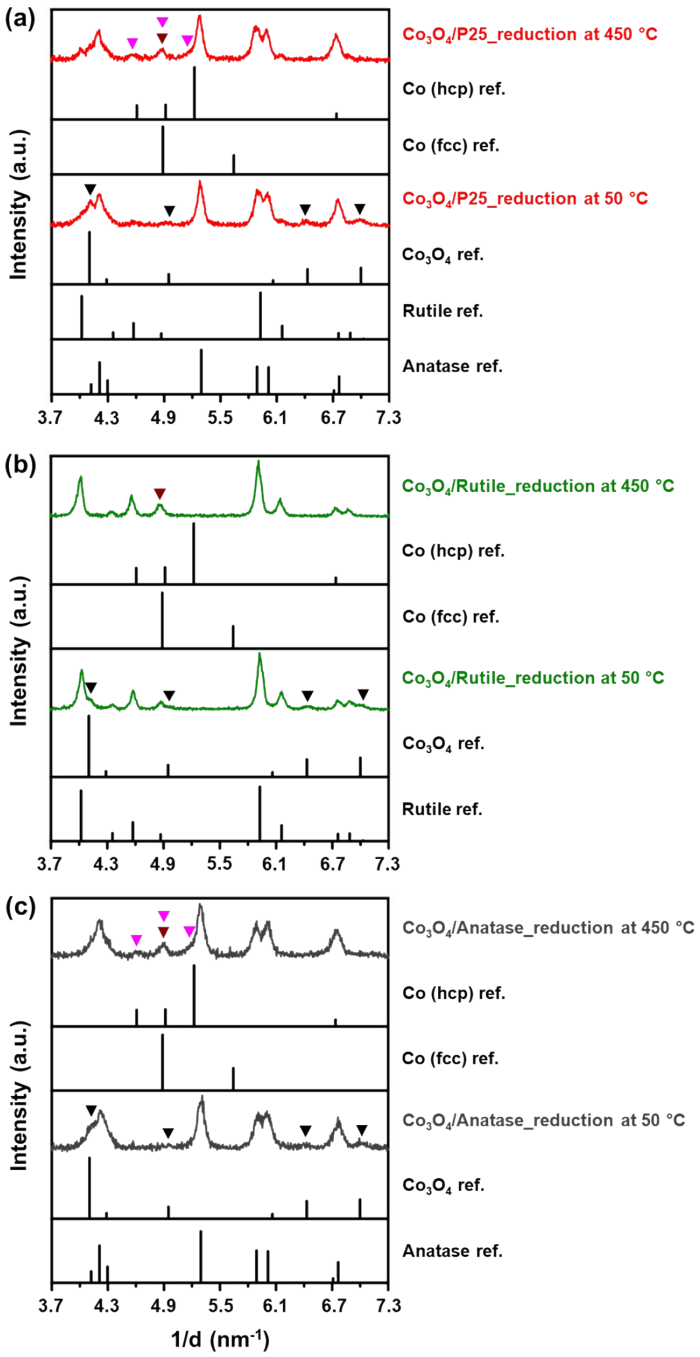

Figure S8: *In situ* PXRD patterns of **(a)** Co_3O_4/P25, **(b)** Co_3O_4/Rutile, and **(c)** Co_3O_4/Anatase recorded at 50 and 450 °C during reduction in a 50:50 H_2:N_2 mixture at atmospheric pressure. The reference reflection lines of metallic Co (fcc and hcp Co^0), Co_3O_4, Rutile, and Anatase are also included. The brown, magenta and black triangles indicate the reflections of fcc Co^0, hcp Co^0, and Co_3O_4, respectively. Note that there exists some overlap between the reflections of the Co-based phases and those of the Rutile and/or Anatase crystal phases.

H_2-TPR profile of Co_3O_4/Anatase and equations for calculating the degree of reduction

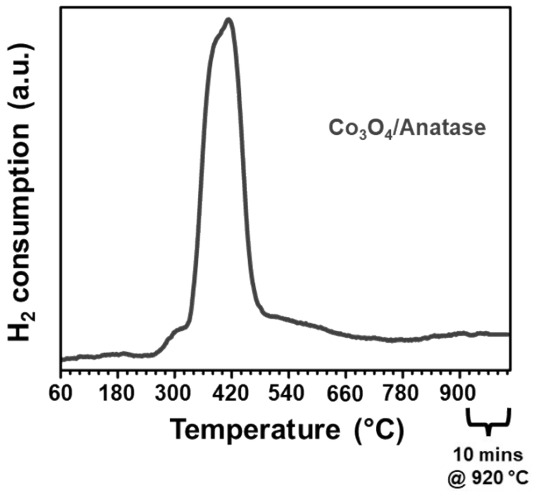

Figure S9: Reduction profile of Co_3O_4/Anatase derived from H_2-TPR performed in a 5:95 H_2:Ar mixture at atmospheric pressure.

In situ PXRD patterns obtained during dry CO-PrOx and magnetometer calibration

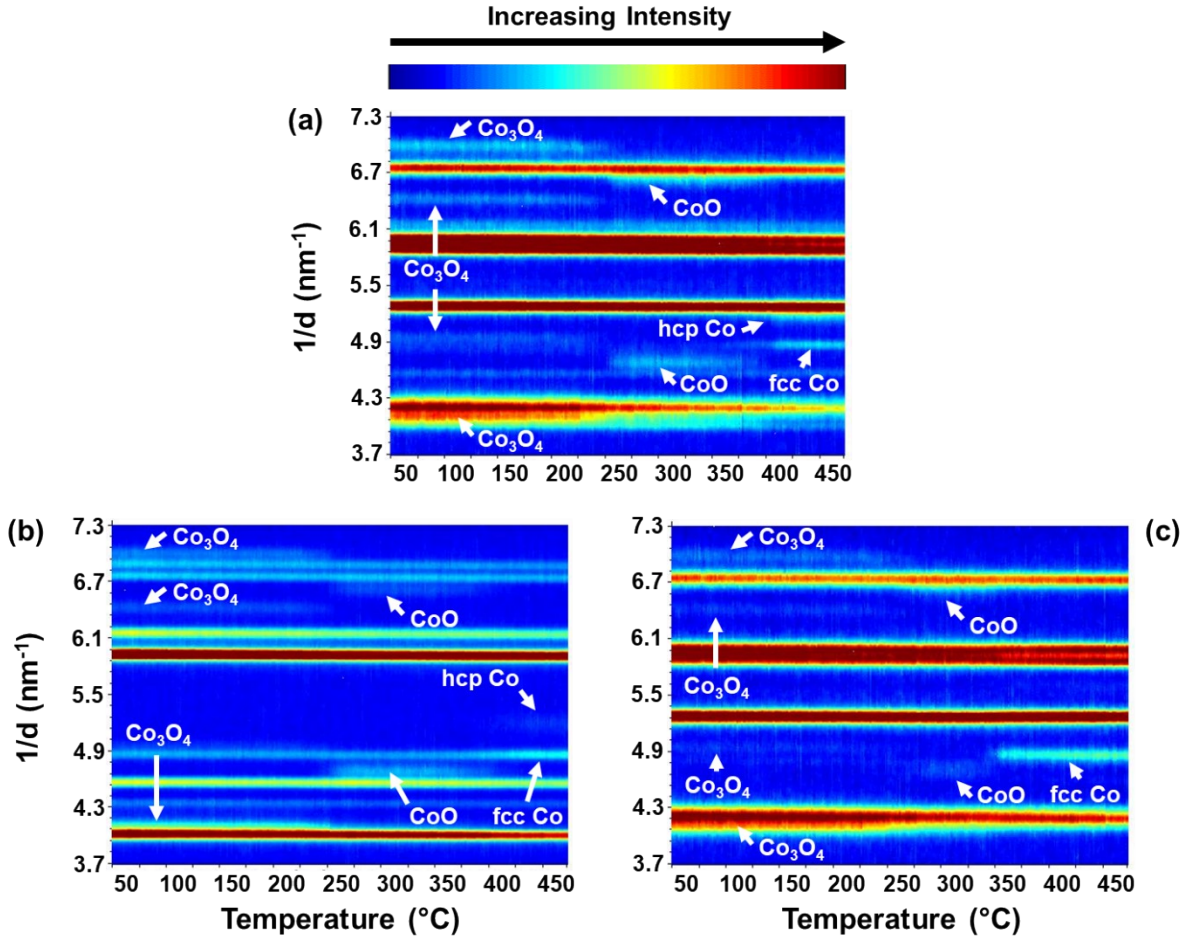

Figure S10: On-top view of the PXRD patterns recorded during dry CO-PrOx over **(a)** Co_3O_4/P25, **(b)** Co_3O_4/Rutile, and **(c)** Co_3O_4/Anatase. (Gas composition: 1% CO, 1% O_2, 50% H_2, 48% N_2; pressure: atmospheric; GHSV: 60000 mL(NTP)/$g_{Co_3O_4}$/h).

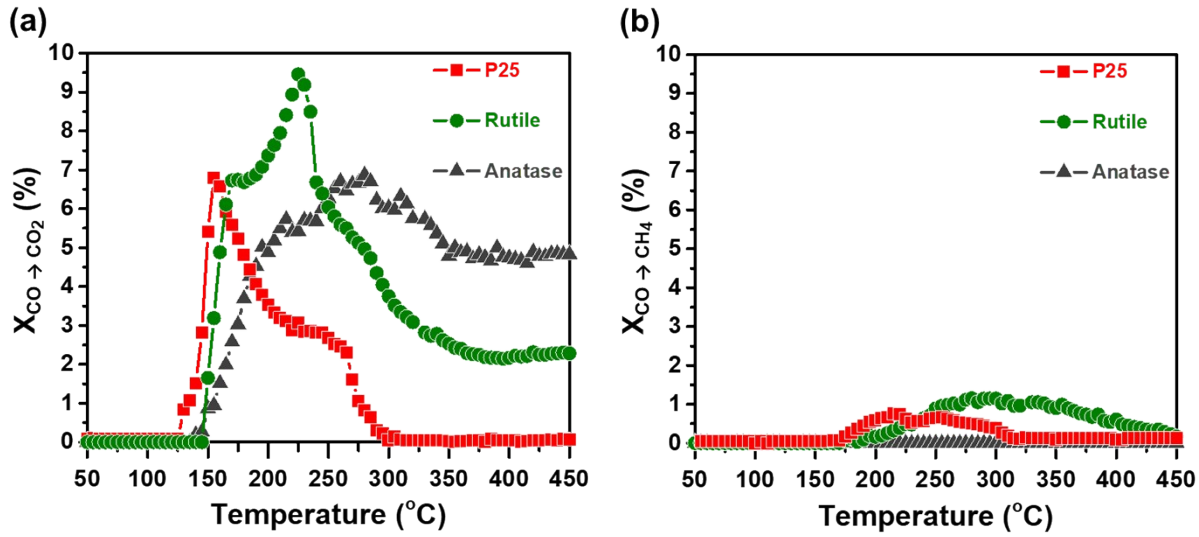

Figure S11: (a) CO conversion to CO_2 ($X_{CO \rightarrow CO_2}$), and **(b)** CO conversion to CH_4 ($X_{CO \rightarrow CH_4}$) during CO-PrOx for all bare supports. (Gas composition: 1% CO, 1% O_2, 50% H_2, and 48% N_2; pressure: atmospheric; GHSV: 60000 mL(NTP)/g_{TiO_2}/h).

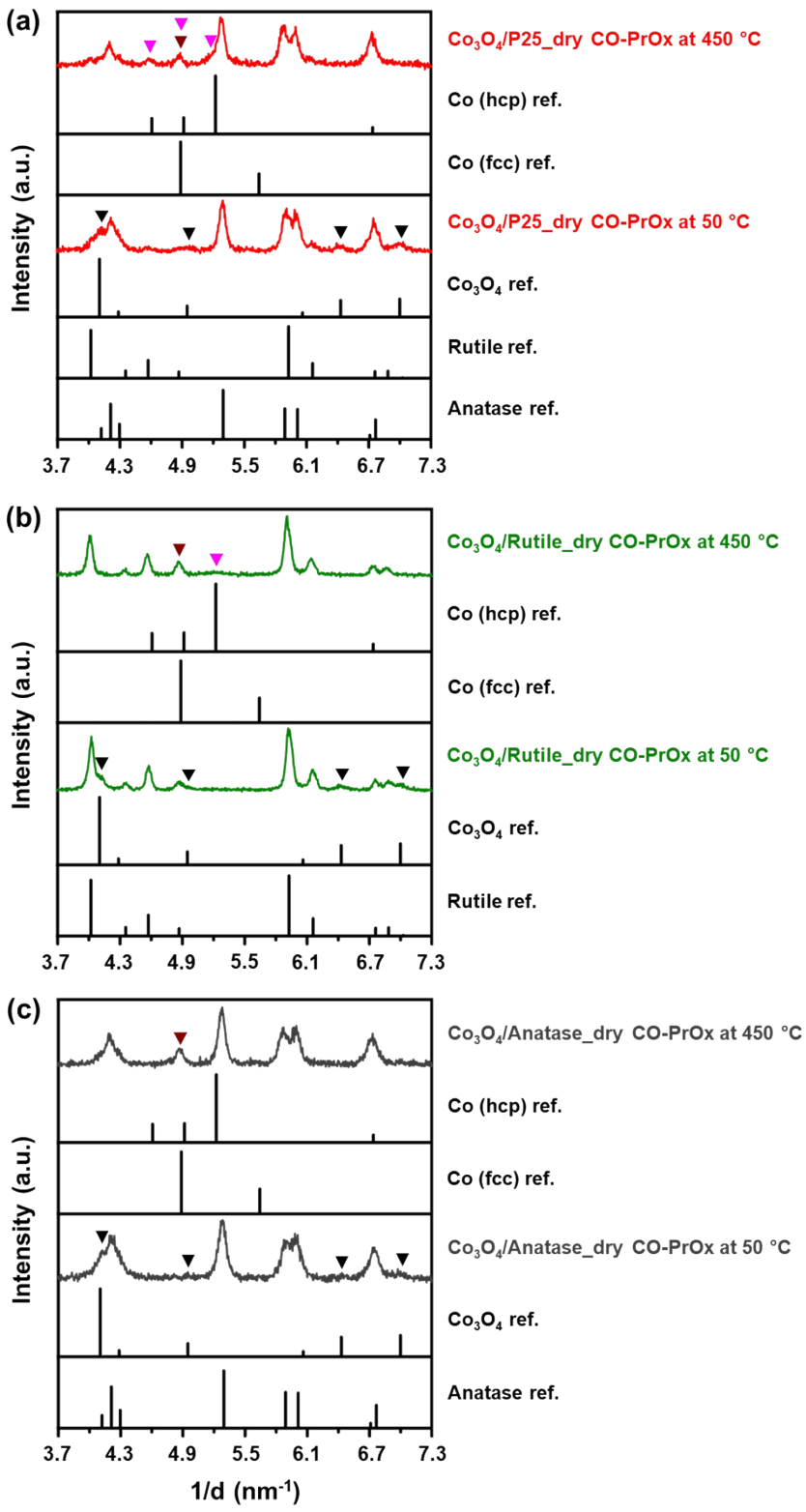

Figure S12: *In situ* PXRD patterns of **(a)** Co_3O_4/P25, **(b)** Co_3O_4/Rutile, and **(c)** Co_3O_4/Anatase recorded at 50 and 450 °C during dry CO-PrOx. The reference reflection lines of metallic Co (fcc and hcp Co^0), Co_3O_4, Rutile, and Anatase are also included. The brown, magenta, and black triangles indicate the reflections of fcc Co^0, hcp Co^0, and Co_3O_4, respectively. Note that there exists some overlap between the reflections of the Co-based phases and those of the Rutile and/or Anatase crystal phases.

Results from thermodynamic calculations: Gibbs free energy and p_{H_2}/p_{H_2O} as a function of temperature

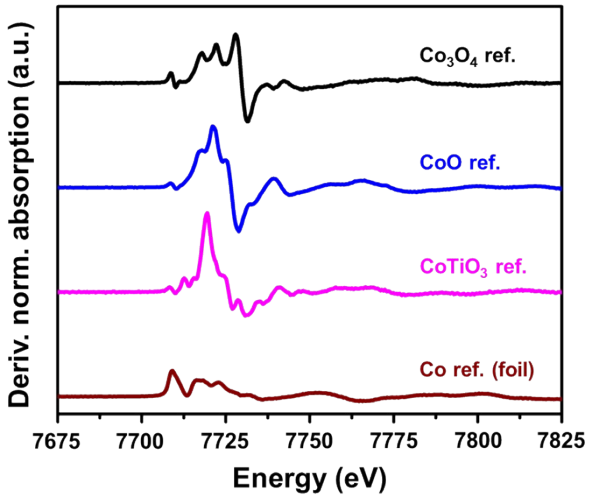

Figure S13: Normalised first derivative XANES spectra of the reference compounds.

Results from thermodynamic calculations: Gibbs free energy and p_{H_2}/p_{H_2O} as a function of temperature

$$Co_3O_4(s) + H_2(g) \rightleftharpoons 3CoO(s) + H_2O(g) \quad (S16)$$

$$Co_3O_4(s) + 4H_2(g) \rightleftharpoons 3Co(s) + 4H_2O(g) \quad (S17)$$

$$Co_3O_4(s) + H_2(g) + 3TiO_2(s) \rightleftharpoons 3CoTiO_3(s) + H_2O(g) \quad (S18)$$

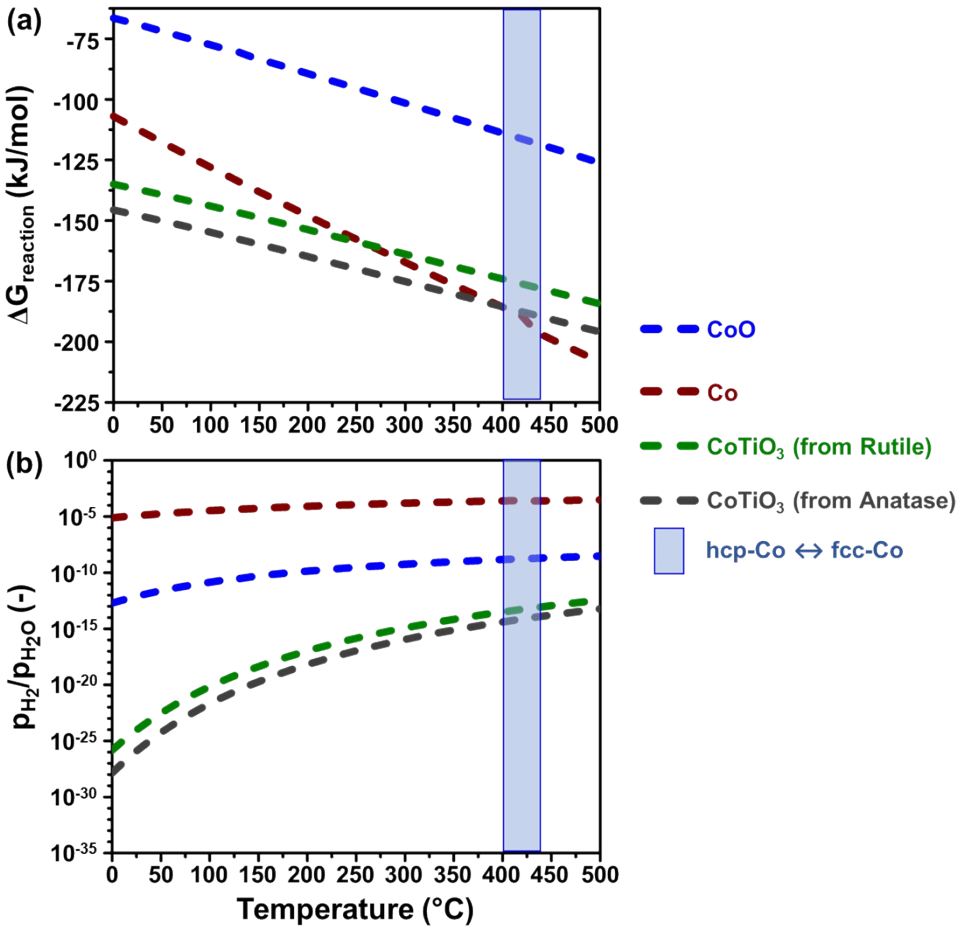

Figure S14: (a) Gibbs free energy and **(b)** p_{H_2}/p_{H_2O} as a function of temperature at 1.013 bar during the reduction of bulk Co_3O_4 to CoO, Co^0, or $CoTiO_3$ (the latter would involve either of the two TiO_2 crystal phases, *viz.*, Anatase or Rutile – see Equation S18), respectively. The light blue shaded area indicates the temperature region where bulk hcp Co^0 transforms into bulk fcc Co^0. Thermodynamic data used in the calculations were obtained from Knacke *et al.*[15]

$$CoO(s) + H_2(g) \rightleftharpoons Co(s) + H_2O(g) \qquad (S19)$$

$$CoO(s) + TiO_2(s) \rightleftharpoons CoTiO_3(s) \qquad (S20)$$

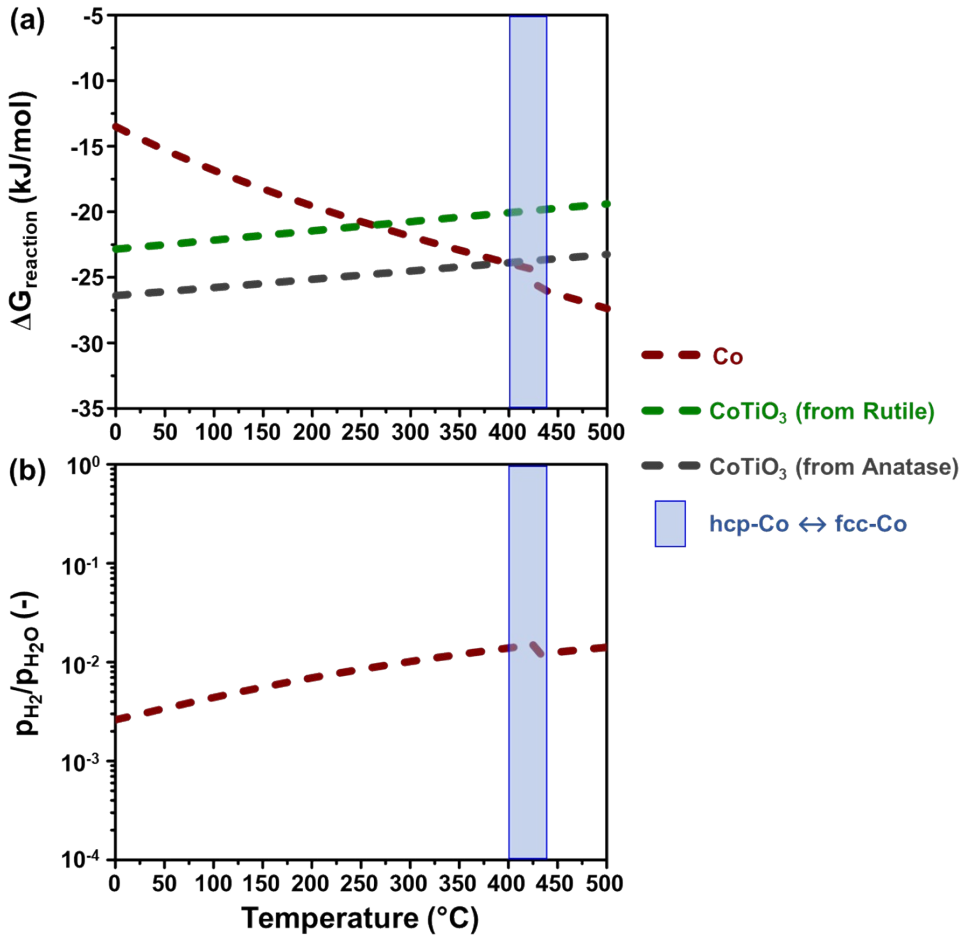

Figure S15: (a) Gibbs free energy as a function of temperature at 1.013 bar during the reduction of bulk CoO forming Co^0 as well as during the solid state-reaction between CoO and TiO_2 (Anatase or Rutile, respectively) forming $CoTiO_3$. Note that the formation of $CoTiO_3$ from CoO does not require H_2 or H_2O (see Equation S20). **(b)** p_{H_2}/p_{H_2O} as a function of temperature at 1.013 bar during the reduction of CoO to Co^0.

Ex situ STEM-EELS analysis of spent catalysts

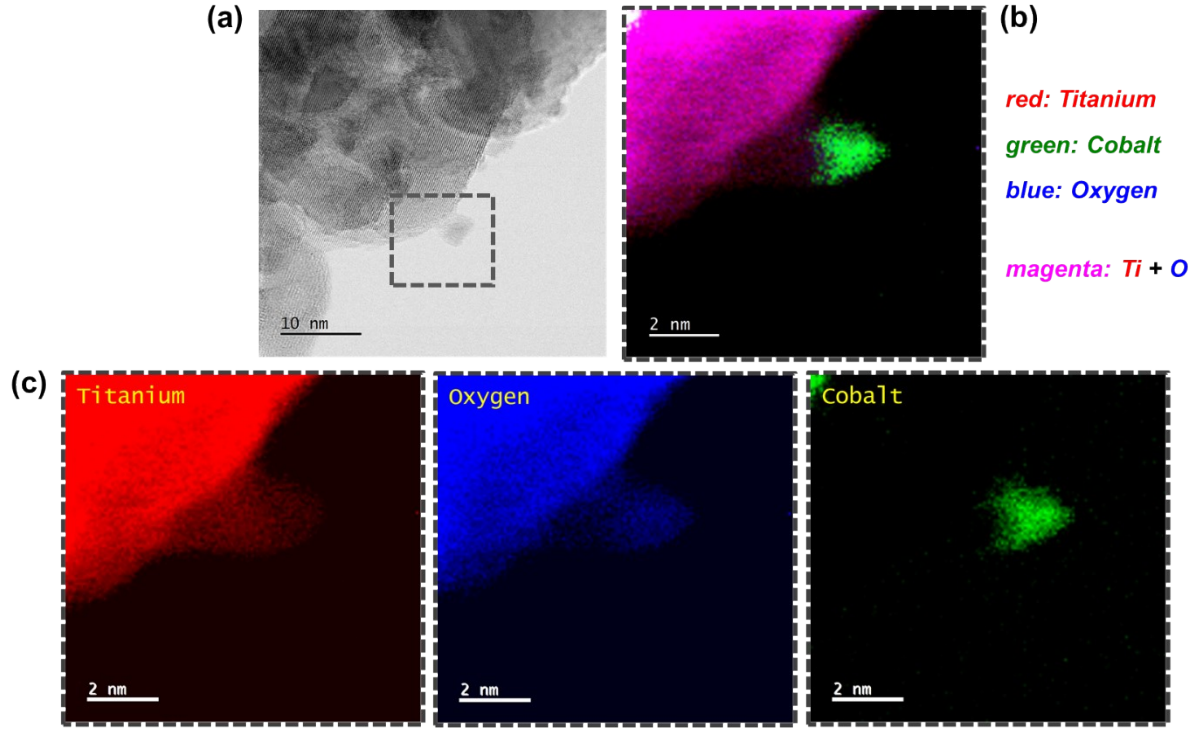

Figure S16: (a) Bright-field STEM micrograph, **(b)** magnified STEM-EELS composite map showing the regions with Ti, O, and Co, and the **(c)** corresponding magnified STEM-EELS maps of the individual elements present in the spent Co_3O_4/Anatase catalyst.

References

1 W. H. Bragg and W. L. Bragg, *Proc. R. Soc. London. Ser. A, Contain. Pap. a Math. Phys. Character*, 1913, **88**, 428–438.

2 ICDD PDF-2 Release 2008 (Database), International Centre for Diffraction Data, Newtown Square, PA, USA, 2008.

3 A. A. Coelho, *J. Appl. Crystallogr.*, 2003, **36**, 86–95.

4 C. A. Schneider, W. S. Rasband and K. W. Eliceiri, *Nat. Methods*, 2012, **9**, 671–675.

5 G. Bergeret and P. Gallezot, in *Handbook of Heterogeneous Catalysis*, eds. G. Ertl, H. Knözinger, F. Schüth and J. Weitkamp, Wiley-VCH Verlag GmbH & Co. KGaA, Weinheim, Germany, 2008, pp. 738–765.

6 A. J. Dent, G. Cibin, S. Ramos, A. D. Smith, S. M. Scott, L. Varandas, M. R. Pearson, N. A. Krumpa, C. P. Jones and P. E. Robbins, *J. Phys. Conf. Ser.*, 2009, **190**, 012039.

7 B. Ravel and M. Newville, *J. Synchrotron Radiat.*, 2005, **12**, 537–541.

8 M. Newville, *J. Synchrotron Radiat.*, 2001, **8**, 322–324.

9 N. Fischer, E. van Steen and M. Claeys, *Catal. Today*, 2011, **171**, 174–179.

10 M. Wolf, N. Fischer and M. Claeys, *Mater. Chem. Phys.*, 2018, **213**, 305–312.

11 M. Wolf, S. J. Roberts, W. Marquart, E. J. Olivier, N. T. J. Luchters, E. K. Gibson, C. R. A. Catlow, J. H. Neethling, N. Fischer and M. Claeys, *Dalton Trans.*, 2019, **48**, 13858–13868.

12 M. C. M. Claeys and N. F. Fischer. Sample Presentation Device for Radiation-Based Analytical Equipment. US Patent 8,597,598 B2, 2013.

13 N. Fischer and M. Claeys, *Catal. Today*, 2016, **275**, 149–154.

14 N. Fischer and M. Claeys, *J. Phys. D. Appl. Phys.*, 2020, **53**, 293001.

15 O. Knacke, O. Kubaschewski and K. Hesselmann, Eds., *Thermochemical properties of inorganic substances*, Springer-Verlag, Berlin, 2nd edn., 1991.